Influence of Tm^{3+} ions on the amplification of Ho^{3+}:$^5I_7 \rightarrow {}^5I_8$ transition in fluoride glass modified by $Al(PO_3)_3$ for applications in mid-infrared optics

Fangwei Qi (祁芳薇)[1], Feifei Huang (黄飞飞)[1,*], Tao Wang (王 涛)[1], Ruoshan Lei (雷若珊)[1], Junjie Zhang (张军杰)[1], Shiqing Xu (徐时清)[1], and Long Zhang (张 龙)[1,2]

[1]*College of Materials Science and Engineering, China Jiliang University, Hangzhou 310018, China*

[2]*Key Laboratory of Materials for High Power Laser, Shanghai Institute of Optics and Fine Mechanics, Chinese Academy of Sciences, Shanghai 201800, China*

**Corresponding author: huangfeifei@cjlu.edu.cn*

Received December 12, 2016; accepted February 17, 2017; posted online March 20, 2017

In this work, we investigate a new type of fluoride glasses modified by $Al(PO_3)_3$ with various Tm^{3+}/Ho^{3+} doping concentrations. The introduced PO_3^- plays an effective role in improving the glass-forming ability and thermal stability. Besides, 1.47, 1.8, and 2.0 μm emissions originating from Tm^{3+} and Ho^{3+}, respectively, are observed. The spectroscopic properties and energy transfer mechanisms between Tm^{3+} and Ho^{3+} are analyzed as well. It is noted that the higher predicted spontaneous transition probability (118.74 s^{-1}) along with the larger product of measured decay lifetime and the emission cross section ($\sigma_{emi} \times \tau$) give evidence of intense 2.0 μm fluorescence.

OCIS codes: 160.4670, 160.5690, 060.2390, 070.4790.

doi: 10.3788/COL201715.051604.

Since the first realization of the 2.0 μm laser output in rare earth (RE) ion Ho^{3+}-doped crystals[1], the 2.0 μm region laser emission is of great interest for its numerous potential applications, including eye-safe LIDAR, medicine, spectroscopy, remote sensing, and mid-infrared (IR) generation[2–6]. Tm^{3+} and Ho^{3+} have been studied as active ions for a laser in this wavelength region in various hosts. Tm^{3+} can create two excited states at the $^3F_4$ state by the cross relaxation (CR) ($^3H_6 + {}^3H_4 \rightarrow {}^3F_4 + {}^3F_4$) energy transfer (ET) process with Tm^{3+}, which is demonstrated to increase quantum efficiency[7]. Compared to Tm^{3+}, Ho^{3+} possesses higher gain cross sections, longer radiative lifetime, and longer-operating laser wavelength. However, the low efficiency of laser action on the Ho^{3+}:$^5I_7 \rightarrow {}^5I_8$ emission limits further applications[8,9]. Otherwise, the lack of a pumping band in the 800 or 980 nm region corresponding to commercially available high-power laser diodes (LDs) was a drawback in Ho^{3+} singly doped systems. In pursuit of efficiency, Ho^{3+}-doped glasses have been sensitized with Tm^{3+}, Yb^{3+}, or Er^{3+}[10–12]. In codoping Tm^{3+} as a sensitizer system, the $^3F_4$ absorption band of Tm^{3+} permitted LD pumping, particularly, combines the effective CR among Tm^{3+}, leading to an increase in quantum efficiency and the effective ET from Tm^{3+} to Ho^{3+} to achieve a Ho^{3+}:$^5I_7 \rightarrow {}^5I_8$ laser, which can be applied to a wider range of applications requiring continuous wave (CW) 2.1 μm laser radiation[13].

In order to obtain a strong IR emission from Ho^{3+}, the host glass matrix is as important as the sensitizer. The early demonstrations of Tm^{3+}/Ho^{3+} codoped fiber lasers involved fluoride glass as the host material[14]. The low-phonon energy, high doping level, low viscosity, and wide transparency from the ultraviolet (UV) to IR of fluoride glasses, allowing for the observation of RE ion-doped laser emissions in a large optical range, make the materials good candidates for applications in laser technology[15]. Fluoroaluminate (AYF) as representatives of fluoride glass are known to show several properties, such as a small refractive index and dispersion, and a high chemical durability implicated for fiber laser practical use, when compared with the properties in other fluoride glass systems. According to previous reports, the addition of some oxides, especially the addition of P_2O_5, is effective in stabilizing the glass state[16]. Moreover, some articles describe properties of fluoride systems in which phosphates were introduced in a form of $NaPO_3$[17], $Ba(PO_3)_2$[18,19], and $Ba(H_2PO_4)_2$[20]. However, fluoride systems with high-doped phosphates are highly similar to fluorophosphate systems, and most studies of fluoride systems focus on structural properties. Therefore, we investigate the fluoride system modified by phosphates in small amounts, especially focusing on the spectral properties of the glass, which has so far been rarely reported.

Based on previous investigations, we studied the physical, chemical, and typical properties, which include the stimulated emission cross section, upper state lifetime for the transition, and absorption spectra for diode laser pumping of Tm^{3+}/Ho^{3+} codoped fluoroaluminate glasses with the introduction of $Al(PO_3)_3$. In addition, the ET processes between Tm^{3+} and Ho^{3+} are analyzed. We look forward to the results of better optical properties along with the advantages of 2.0 μm laser output.

In this work, the AYF glasses had the composition of $95(AlF_3 - YF_3 - MgF_2 - CaF_2 - SrF_2 - BaF_2)-$

$5Al(PO_3)_3 - xTmF_3 - yHoF_3$ ($x = 0.2$, $y = 0$, 0.1, 0.2, 0.3, 0.4, singed as TH0, TH1, TH2, TH3, TH4; $y = 0.2$, $x = 0$, 0.1, 0.2, 0.3, 0.4, singed as HT0, HT1, HT2, HT3, HT4, respectively). Commercial grade chemicals of fluoride were used as starting materials. Approximately 15 g doped glass batches of different compositions were melted in an alumina crucible at 950°C for 20 min with a closed lid for each batch, and then the melts were poured onto a preheated copper plate and annealed near the glass transition temperature for several hours. The glass samples were fabricated and polished to the size of 20 mm × 10 mm × 1 mm for the optical property measurements after it naturally cooled down to room temperature, and a part of the milled glass sample was used for the differential scanning calorimetry (DSC). Through the Archimedes principle, the densities were tested using distilled water as the immersion liquid. The density was measured to be 3.73 ± 0.01 g/cm^3, and the refractive index of the glass was calculated to be 1.64.

The DSC was measured using a NETZSCH DTA 404 PC at the heating rate of 15 K/min. The absorption spectra were recorded on a JASCOV 570UV/VIS spectrophotometer in the range of 400-2200 nm at room temperature. The fluorescence spectra were obtained with a computer-controlled Triax 320 spectrofluorimeter with a 1.5 W 808 nm LD using a PbSe detector. The fluorescence lifetime was determined by a combined fluorescence lifetime and a steady state spectrometer (FLSP 920) (Edingburg Co.). The Raman spectrum of the glass was measured with a Renishaw in Via Raman microscope in the 100–1000 cm^{-1} spectrum range using a 532 nm excitation line.

Glass stability versus devitrification may be estimated from the characteristic temperatures, including glass transition temperature (T_g), crystallization onset temperature (T_x), and the peak temperature of crystallization (T_p) measured by the DSC, and the results are shown in the Fig. 1. In some cases, the assessments may be not always accurate, and the ΔT difference between the T_g and the T_x is widely believed to have the value is strongly correlated to the crystallization tendency. A large ΔT means strong inhibitions to the processes of nucleation and crystallization[21], which reflects greater thermal stability of the glass. In the Fig. 1, the T_g and T_x are noted as a value of 456°C and 560°C, respectively, and ΔT is calculated as 104°C, which is higher than the value of 81°C of the reported AYF glass[22]. Moreover, the value calculated by the formula $k_{gl} = (T_x - T_g)/(T_m - T_p)$ is developed as a new parameter to judge glass formation[21], and the higher one reflects the greater thermal stability of the glass, where T_m is the melting temperature of the glass. The k_{gl} is figured out to be 0.297 in this $Al(PO_3)_3$-doped AYF glass system, and larger than the previous value of 0.171 in the AYF system without $Al(PO_3)_3$[22], which reveals a better glass-forming ability and chemical durability.

In order to investigate the structural properties of the AYF glass modified by $Al(PO_3)_3$, the Raman spectrum of the prepared sample of undoped RE ion glass is shown in Fig. 1. A peak in the low-frequency Raman band around 560 cm^{-1} is observed clearly, which is related to [AlF_4] vibration[23,24]. A band at 1090 cm^{-1} is due to the stretching vibration of O-P-O after introducing the metaphosphate into the AYF glass[23].

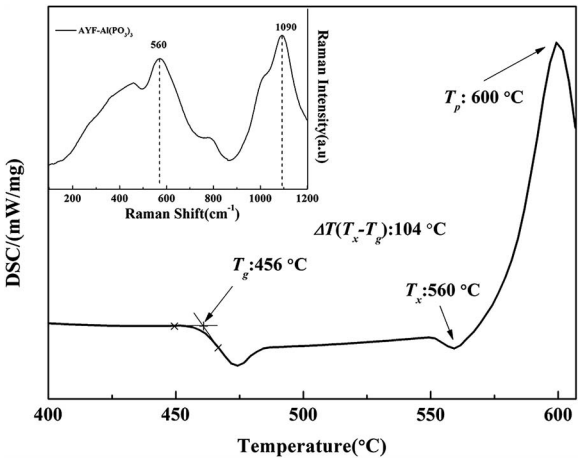

Fig. 1. DSC curve of the AYF glass with 5 mol% $Al(PO_3)_3$ introduction. Raman spectrum in the 100–1200 cm^{-1} range of undoped RE ions AYF glass with $Al(PO_3)_3$ introduction.

The IR absorption spectra of the Tm^{3+} and Ho^{3+} singly doped, respectively, and Tm^{3+}/Ho^{3+} codoped AYF glasses modified by $Al(PO_3)_3$ at room temperature between 400–2200 nm are shown in Fig. 2. The spectral absorption peak shapes of all of the samples are similar, and the absorption intensity is proportional to the doping concentrations, indicating that Tm^{3+} and Ho^{3+} are uniformly incorporated into the glassy network and do not cause aggregation or local ligand field variations[25]. The absorption bands of Ho^{3+} including 449, 544, 641, 1149, and 1944 nm correspond to the transitions from the

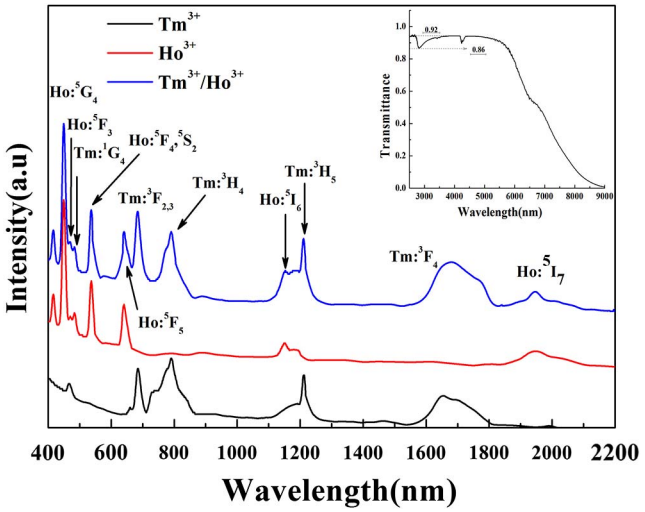

Fig. 2. Absorption spectra of Tm^{3+} and Ho^{3+} singly doped and codoped samples. The inset is the transmittance spectrum of the sample.

$^5I_8$ ground state to the higher levels $^5F_3$, ($^5F_4$, $^5S_2$), $^5F_5$, $^5I_6$, and $^5I_7$, as is labeled, respectively, in the Fig. 2. It can be seen from Fig. 2 that no absorption peak exists in the Ho^{3+} single-doped AYF glass with an $Al(PO_3)_3$ introduction in the range of 750–850 nm, while the absorption of Tm^{3+}, corresponding to the optical transition $^3H_6 \rightarrow {}^3H_4$, can be observed. It indicates that Tm^{3+} can be effectively excited by the 808 nm pumping source, and Ho^{3+} can be sensitized effectively through an ET.

The inset of Fig. 2 presents the mid-IR transmittance spectrum of Tm^{3+}/Ho^{3+} codoped AYF modified by the $Al(PO_3)_3$ sample. As it can be seen, the maximum transmittance reaches as high as 92%. As we know, the stretching vibration of free OH^- groups will participate in the ET of RE ions and reduce the intensity of the emission[26]. The content of the OH^- groups in the glass can be expressed by the OH^- absorption coefficient, which can be given by

$$\alpha_{OH^-} = \mathrm{In}(T/T_0)/l, \tag{1}$$

where l is the thickness of the sample (1 mm), and T_0 and T are the transmitted and incident intensities, respectively. The absorption coefficient at 3 μm is 0.067 cm^{-1}, which is much lower than 0.113 cm^{-1} of the AYF original glass[22]. The good mid-IR transmission property proves that AYF glass modified by $Al(PO_3)_3$ is a potential candidate for mid-IR laser materials.

The Judd-Ofelt (J-O) parameter $\Omega_\lambda(\lambda = 2, 4, 6)$ based on the J-O theory is used to analyze the local structure and bonding in the vicinity of RE ions[27,28]. According to the absorption spectrum (Fig. 2), the $\Omega_\lambda\,(\lambda = 2, 4, 6)$ of Ho^{3+} within various glasses are calculated (shown in Table 1)[29,30]. The parameter, Ω_2, is hypersensitive to structure, which is related to the covalency parameter through the nephelauxetic effect and polarizability of the ligands around RE ions[31]. It is seen that Ω_2 of the AYF glass modified by $Al(PO_3)_3$ is slightly larger than fluoride, but much smaller than oxide glasses, which indicates that the present sample glasses possess a lower covalency and a higher symmetry of the ligand, owing to the O^{2-} ions introduction owning a higher polarizability than F^- ions. Ω_6 is a vibronic dependent parameter, which is related to viscosity, rigidity, and the dielectric. Ω_4/Ω_6 is an important parameter for predicting the stimulated emission in a laser active host[32]; in this work, the value of Ω_4/Ω_6 is 2.04. The root-mean-square error deviation δ_{rms} is 0.18×10^{-6} for Tm^{3+}/Ho^{3+} codoped AYF glass modified by $Al(PO_3)_3$.

The radiative parameters, radiative transition probability (A), branching ratio (β), total radiative transition probability (ΣA), and radiative lifetime (τ_{rad}) of Ho^{3+} in the 0.3 mol% Tm^{3+}/0.2 mol% Ho^{3+} (HT3) sample are calculated according to Ω_λ (presented in Table 2). From Table 2, A of the Ho^{3+}: $^5I_7 \rightarrow {}^5I_8$, $^5I_5 \rightarrow {}^5I_8$, and $^5I_5 \rightarrow {}^5I_8$ transitions in the AYF glass modified by $Al(PO_3)_3$, are as high as 118.74 ± 0.1, 254.46 ± 0.1, and 3490.34 ± 0.1 s^{-1}, respectively, which are higher than the values of 61.44, 135.59, and 2242.06 s^{-1} in other kinds of fluoride glass[33]. Thus, this Tm^{3+}/Ho^{3+} codoped AYF glass modified by $Al(PO_3)_3$ can be selected as an appropriate host material to achieve a stronger 2.0 μm fluorescence on account of its high spontaneous emission probability, which means a better opportunity of obtaining laser actions[34].

Figure 3 presents the fluorescence spectra of the prepared Tm^{3+}/Ho^{3+} codoped glass samples with various Tm^{3+} or Ho^{3+} molar concentrations in the wavelength region of 1350–2200 nm. The inset of Fig. 3 shows the simplified energy level diagram of the Tm^{3+}/Ho^{3+} codoped system. The 808 nm pump source excites the Tm^{3+} from the $^3H_6$ ground state to the higher $^3H_4$ level. On the one hand, a portion of the Tm^{3+} ions at the $^3H_4$ level decay to the $^3F_4$ meta-stable level by radiative transition emitting 1.47 μm photons, and then returns to the ground state with a strong 1.8 μm emission via the $^3F_4 \rightarrow {}^3H_6$ transition. On the other hand, another part of the Tm^{3+} ion at the $^3H_4$ level can also transfer energy to the $^3H_6$ ground state and decay rapidly to the $^3F_4$ level via the CR process $Tm^{3+}(^3H_4) + Tm^{3+}(^3H_6) \rightarrow Tm^{3+}(^3F_4) + Tm^{3+}(^3F_4)$. Then, the Tm^{3+} located at the $^3F_4$ level transfers energy to the neighboring ground state of Ho^{3+} by the ET process $Tm^{3+}(^3F_4) + Ho^{3+}(^5I_8) \rightarrow Tm^{3+}(^3H_6) + Ho^{3+}(^5I_7)$, so that a mid-IR fluorescence emission of 2.0 μm associated with the Ho^{3+}:$^5I_7 \rightarrow {}^5I_8$ transition takes place. In the Fig. 3(a), the concentration of Ho^{3+} is increased using values 0.1, 0.2, 0.3, and 0.4 mol%, while the concentration of Tm^{3+} remains fixed at 0.2 mol%. It can be seen that the fluorescence intensity at 1.47 μm is almost consistent, which is caused by two ET processes that may counteract each other to a certain

Table 1. J-O Parameters Ω_λ of Ho^{3+} in Various Glasses

$\Omega_\lambda(\times 10^{-20}$ $cm^2)$	Ω_2	Ω_4	Ω_6	Ω_4/Ω_6	Reference
Fluoride	1.86	1.90	1.32	1.43	[29]
Phosphate	5.60	2.72	1.87	1.45	[29]
Silicate	5.84	2.38	1.75	1.36	[30]
AYF-$Al(PO_3)_3$	2.22 ± 0.02	3.85 ± 0.04	1.88 ± 0.02	2.04	Present
δ_{rms}	0.18×10^{-6}				

Table 2. Predicted Spontaneous Transition Probability (A), Total Spontaneous Transition Probability (ΣA), Branching Ratios (β), and Radiative Lifetimes (τ_{rad}) of AYF Glass Modified by $Al(PO_3)_3$ for Various Selected Excited Levels of Ho^{3+}

Transition	λ (nm)	$A(s^{-1})$	$\Sigma A(s^{-1})$	β	τ (ms)
$^5I_7 \rightarrow {}^5I_8$	1944	118.74	118.74 ± 0.1	$100.00\% \pm 0.2\%$	8.42
$^5I_6 \rightarrow {}^5I_8$	1152	215.09	254.46	84.53%	3.93
$^5I_7$	2810	39.37		15.47%	
$^5I_5 \rightarrow {}^5I_8$	887	81.16	204.12	39.76%	4.90
$^5I_7$	1631	107.73		52.78%	
$^5I_6$	3890	15.23		7.46%	
$^5I_4 \rightarrow {}^5I_8$	757	10.95	111.26	9.84%	8.99

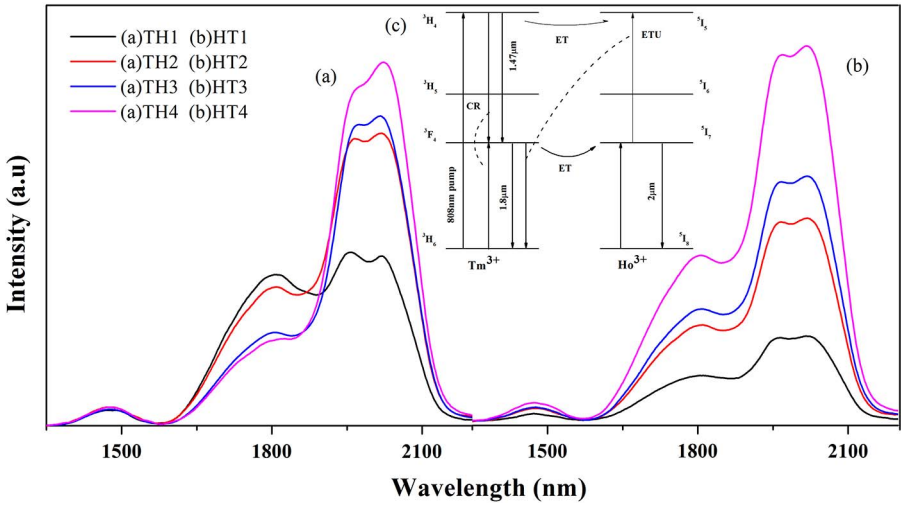

Fig. 3. Fluorescence spectra of Tm^{3+}/Ho^{3+} codoped AYF glass modified by $Al(PO_3)_3$ with (a) different Ho^{3+} concentrations and (b) different Tm^{3+} concentrations. (c) The inset shows the energy level scheme of the Tm^{3+}/Ho^{3+} system. ETU, ET upconversion.

extent. For one thing, the increase of Ho^{3+} facilitates the ET of Tm^{3+}:$^3H_4 \rightarrow Ho^{3+}$:$^5I_5$, which leads to the decrease of 1.47 μm fluorescence. For another, the CR among Tm^{3+} is weakened by the enlargement of the distance among Tm^{3+} due to the addition of Ho^{3+}, which results in a 1.47 μm fluorescence enhancement. The two processes reach equilibrium so that the fluorescence intensity at 1.47 μm remains constant. In contrast, the intensity of 1.8 μm is limited to the numbers of Tm^{3+} staying on the $^3F_4$ level. As the Ho^{3+} concentration increases, most of the Tm^{3+} are transported to the $^5I_7$ level, making for a 1.8 μm fluorescence reduction and a 2.0 μm fluorescence enhancement, which proves the effective ET of Tm^{3+}: $^3F_4 \rightarrow Ho^{3+}$:$^5I_7$ and without concentration quenching happening. From Fig. 3(b), it is worth noting that the emission intensities at 1.47, 1.8, and 2.0 μm show increases of various degrees with the increment of Tm^{3+} concentration, and the intensity reaches the maximum when Tm^{3+} increases to 0.4 mol%, which can be attributed to the CR mechanism. According to the above results, a conclusion can be drawn that the sensitization effect of Tm^{3+} on Ho^{3+} is significant and simultaneous, and the strong fluorescence for the $^3H_4 \rightarrow {}^3H_6$ transition of Tm^{3+} can still be observed at lower Ho^{3+} concentrations.

Figure 4(a) shows the decay curve of the Ho^{3+} in the HT series. The experimental lifetimes of the 2.0 μm emission turn out to be 1.72, 2.02, 2.53, and 2.86 ms, respectively. The result indicates that the lifetime of Ho^{3+} increases after, meanwhile, the ET efficiency η from Tm^{3+} to Ho^{3+} can be determined from the lifetime value by using the following formula[29]:

$$\eta = 1 - \frac{\tau}{\tau_0}, \tag{2}$$

where τ_0 and τ are the lifetimes of Tm^{3+}:$^3F_4$ level in Tm^{3+} singly doped and Tm^{3+}/Ho^{3+} codoped samples, respectively. The ET efficiency of the TH1-4 samples, where the Tm^{3+} concentration was fixed at 0.2 mol%, are shown in the Fig. 4(b). It can be seen that the ET efficiency

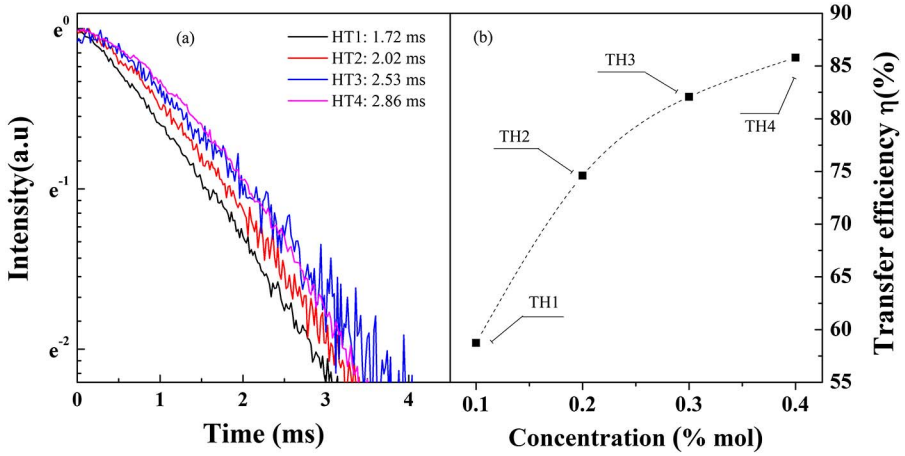

Fig. 4. (a) decay curves of Ho^{3+} in the HT1-4 samples, where the Ho^{3+} concentration is fixed at 0.2 mol% and (b) ET efficiencies from Tm^{3+} to Ho^{3+} in the TH1-4 samples.

increases with an increasing Ho^{3+} concentration and reaches a maximum of 88% when the Ho^{3+} concentration is up to 0.4 mol%. Tm^{3+} is codoped with a constant increase concentration, which concurs with the result of the fluorescence spectra. Thus, efficient ET from Tm^{3+} to Ho^{3+} can be obtained efficiently in the present glass, which is helpful in 2.0 μm emission.

According to the measured absorption spectra shown in Fig. 3, the absorption cross section (σ_{abs}) can be calculated via the following equation[35]:

$$\sigma_{\mathrm{abs}}(\lambda) = \frac{2.303 \log\left[\frac{I_0(\lambda)}{I(\lambda)}\right]}{Nl}, \tag{3}$$

where $I_0(\lambda)$ and $I(\lambda)$ are the incident optical intensity and optical intensity throughout the sample, respectively. N is the concentration of Ho^{3+}, and l is the thickness of the sample. Moreover, on the basis of the obtained absorption cross section, the stimulated emission cross section (σ_{emi}), which is an extremely useful parameter to determine the possibility of achieving the laser effect is further calculated by using the McCumber formula[36],

$$\sigma_{\mathrm{emi}}(\lambda) = \sigma_{\mathrm{abs}}(\lambda)\frac{Z_l}{Z_u}\exp\left[\frac{hc}{kT}\left(\frac{1}{\lambda_{\mathrm{ZL}}} - \frac{1}{\lambda}\right)\right], \tag{4}$$

where h, c, k, and T are the Planck constant, the photon frequency, the Boltzmann constant, and the temperature (the room temperature in this case). Z_l and Z_u are the partition functions of the lower and upper levels, respectively. Z_l/Z_u simply becomes the degeneracy weighting of the $^5I_7$, $^5I_8$ states in the high-temperature limit, hence, the value is equal to 1.13. λ_{ZL} is the wavelength for the transition between the lower Stark sublevels of the emitting multiplets and the lower Stark sublevels of the receiving multiplets (zero phonon line). As shown in Fig. 5, both the absorption and emission cross sections of the Ho^{3+}:$^5I_8 \rightarrow {}^5I_7$ transition are shown, and the maximum values of them at

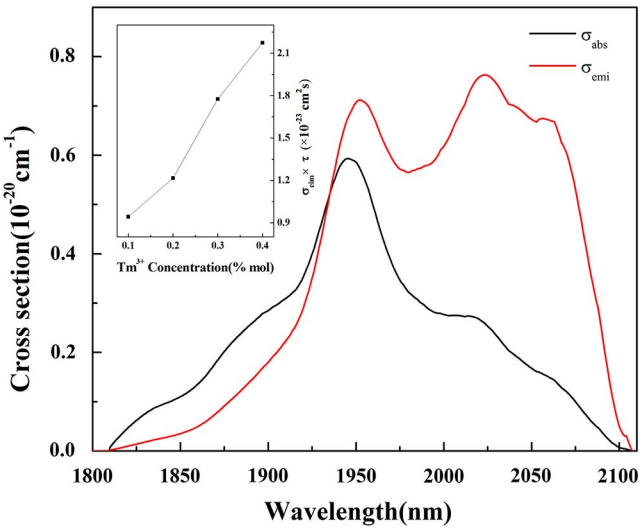

Fig. 5. Absorption cross section and emission cross section of the Ho^{3+}:$^5I_8 \rightarrow {}^5I_7$ transition in the HT4 sample at the 2.0 μm region. The inset shows the products of the emission cross section and measured decay lifetime ($\sigma_{\mathrm{emi}} \times \tau$) in the HT1-4 samples.

2.0 μm are 5.9×10^{-21} and 7.6×10^{-21} cm^{-2}, respectively. The result is preferable to that of various rare-earth-ion-doped glasses, as shown in Table 3[20,31,37–40], thus this AYF glass modified by $Al(PO_3)_3$ is considered to be suitable for IR emission. The products of full width at half maximum (FM) and emission cross section (FM × σ_{emi}) and emission cross section and measured decay lifetime ($\sigma_{\mathrm{emi}} \times \tau$) are important parameters used in optical amplifiers to evaluate bandwidth properties and gain properties, respectively. The FM × σ_{emi} and $\sigma_{\mathrm{emi}} \times \tau$ are, respectively, calculated values of 145.35×10^{-20} cm^2 nm and 2.17×10^{-20} cm^2 s of the HT4 sample. Both of the values are higher than those of 124.80×10^{-20} cm^2 nm and 1.84×10^{-20} cm^2 s in fluorophosphate glasses[3].

In conclusion, Tm^{3+}/Ho^{3+} codoped AYF glass with an $Al(PO_3)_3$ introduction, possessing higher thermal stability against crystallization, is investigated, and the introduced

Table 3. σ_{emi} of 2.0 μm of Ho^{3+} in Various RE-Ion-Doped Glasses

Ions	Glass	σ_{emi} (10^{-21} cm^{-2})	Reference
Tm^{3+}/Ho^{3+}	AYF-$Al(PO_3)_3$	7.60	Present work
	Fluorophosphate	6.15	[31]
	Silicate	3.07	[37]
Yb^{3+}/Ho^{3+}	Fluorophosphate	4.53	[20]
	Silicate	5.05	[38]
$Yb^{3+}/Tm^{3+}/Ho^{3+}$	Phosphate	4.21	[39]
	Fluorophosphate	5.50	[40]

PO_3^- plays an effective role in improving the glass-forming ability. We investigate the fluorescence at 1.47, 1.8, and 2.0 μm with emission performances and ET characteristics by a series of doping concentrations of RE ions. The conclusion can be drawn that Ho^{3+} produces a strong 2.0 μm fluorescence with the help of the sensitization of Tm^{3+}. Besides, the fluorescence intensity of 1.8 μm decreases, while at the same time the 2.0 μm fluorescence intensity adds up with the increase of Ho^{3+} with no concentration quenching occuring in this case. It can be speculated that intensity of the 2.0 μm emission can be significantly increased by highly doping RE ions. The higher products of FM $\times$ σ_{emi} and $\sigma_{emi} \times \tau$ prove that the new AYF glass can achieve high gains when used in the laser amplifier. The results indicate that Tm^{3+}/Ho^{3+} codoped AYF glass modified by $Al(PO_3)_3$ could be a promising material for a widely tunable laser or broadband amplifier applications.

This work was supported by the National Natural Science Foundation of China (Nos. 61605192 and 51401197) and the Open Fund of the Guangdong Engineering Technology Research and Development Center of Special Optical Fiber Materials and Devices (South China University of Technology).

References

1. L. F. Johnson, G. D. Boyd, and K. Nassau, J. Proc. IRE **50**, 87 (1962).
2. X. L. Zou and H. Toratani, J. Non-Cryst. Soilds. **195**, 113 (1996).
3. Y. Tian, L. Zhang, R. Xu, L. Hu, and J. Zhang, Appl. Phys. B. **101**, 861 (2010).
4. S. Vyas, T. Tanabe, M. Tiwari, and G. Singh, Chin. Opt. Lett. **14**, 123201 (2016).
5. Z. Zhang, D. Y. Shen, A. J. Boyland, J. K. Sahu, W. A. Clarkson, and M. Ibsen, Opt. Lett. **33**, 2059 (2008).
6. D. Theisen-Kunde, V. Ott, R. Brinkmann, and R. Keller, Med. Laser. Appl. **22**, 139 (2007).
7. M. Li, G. Bai, Y. Guo, L. Hua, and J. Zhang, J. Lumin. **132**, 1830 (2012).
8. F. Huang, J. Cheng, and X. Liu, Opt. Express. **22**, 20924 (2014).
9. D. C. Hanna, R. M. Percival, R. G. Smart, J. E. Townsend, and A. C. Tropper, Electron. Lett. **25**, 593 (1989).
10. R. Chen, Y. Tian, B. Li, X. Jing, and J. Zhang, Photon. Res. **4**, 214 (2016).
11. G. Bai, Y. Guo, L. Hu, and J. Zhang, Opt. Mater. **33**, 1316 (2011).
12. P. Guan, X. Fan, W. Li, and X. Liu, Chin. Opt. Lett. **14**, 081601 (2016).
13. S. D. Jackson and S. Mossman, Appl. Phys. B. **77**, 489 (2003).
14. J. Y. Allain, M. Monerie, and H. Poignant, Electron. Lett. **27**, 1513 (1991).
15. Y. Tian, J. Zhang, X. Jing, Y. Zhu, and S. Xu, J. Lumin. **138**, 94 (2013).
16. I. Yasui, H. Hagihara, and H. Inoue, J. Non-Cryst. Solids. **140**, 130 (1992).
17. T. Djouama, A. Boutarfaia, and M. Poulain, J. Phys. Chem. Solids. **69**, 2756 (2008).
18. A. Mallik and B. Pal, Mater. Sci. Eng. B. **179**, 77 (2014).
19. B. Karmakar, P. Kundu, and R. N. Dwivedi, Mater. Lett. **57**, 953 (2002).
20. H. Chen, F. Chen, T. Wei, Q. Liu, R. Shen, and Y. Tian, Opt. Commun. **321**, 183 (2014).
21. N. H. Chan, R. K. Sharma, and D. M. Smyth, J. Am. Ceram. Soc. **65**, 167 (1982).
22. F. Huang, Y. Ma, and W. Li, Sci. Rep. **4**, 3607 (2014).
23. R. Lebullenger, L. A. O. Nunes, and A. C. Hernandes, J. Non-Cryst. Soilds. **284**, 55 (2001).
24. U. Gross, S. Riidiger, E. Keminitz, K. Brzezinka, S. Mukhopadhyay, C. Bailey, A. Wander, and N. Harrision, J. Phys. Chem. A. **111**, 5813 (2007).
25. H. Ebendorff-Heidepriem, I. Szabo, and Z. Rasztovits, Opt. Mater. **14**, 127 (2000).
26. G. Wang, S. Dai, J. Zhang, S. Xu, L. Hu, and Z. Jiang, J. Non-Cryst. Solids. **351**, 2147 (2005).
27. B. R. Judd, Phys. Rev. **127**, 750 (1962).
28. G. S. Ofelt, J. Chem. Phys. **37**, 511 (1962).
29. B. Peng and T. Izumitani, Opt. Mater. **4**, 797 (1995).
30. P. R. Watekar, S. Ju, and W. T. Han, J. Non-Cryst. Solids. **354**, 1453 (2008).
31. Y. Tian, R. Xu, L. Hu, and J. Zhang, J. Appl. Phys. **108**, 083504 (2010).
32. F. Huang, Y. Guo, Y. Ma, L. Zhang, and J. Zhang, Appl. Opt. **52**, 1399 (2013).
33. F. Huang, J. Cheng, X. Liu, L. Hu, and D. Chen, Opt. Express. **22**, 20924 (2014).
34. J. Heo, Y. B. Shin, and J. N. Jang, Appl. Opt. **34**, 4284 (1995).
35. G. Chen, Q. Zhang, G. Yang, and Z. Jiang, J. Fluoresc. **17**, 301 (2007).
36. D. E. McCumber, Phys. Rev. **134**, A299 (1964).
37. M. Li, Y. Guo, G. Bai, Y. Tian, L. Hu, and J. Zhang, J. Quant. Spectrosc. Ra. **127**, 70 (2013).
38. R. Cao, M. Cai, Y. Lu, and Y. Tian, Appl. Opt. **55**, 2065 (2016).
39. Y. Tian, R. Xu, L. Hu, and J. Zhang, J. Appl. Phys. **110**, 033502 (2011).
40. L. Yi, M. Wang, S. Feng, Y. Chen, G. Wang, L. Hu, and J. Zhang, Opt. Mater. **31**, 1586 (2009).